Formation of spinel from olivine

Zongwen Liu, Patrick M. Kelly, John Drennan, Peter Mora, and Hisao Kanda

Citation: Applied Physics Letters **84**, 1856 (2004); doi: 10.1063/1.1675939

View online: http://dx.doi.org/10.1063/1.1675939

View Table of Contents: http://scitation.aip.org/content/aip/journal/apl/84/11?ver=pdfcov

Published by the AIP Publishing

Formation of spinel from olivine

Zongwen Liu[a] and Patrick M. Kelly
Department of Mining, Minerals & Materials Engineering, The University of Queensland, Brisbane 4072, Australia

John Drennan
Center for Microscopy and Microanalysis, The University of Queensland, Brisbane 4072, Australia

Peter Mora
Queensland University Advanced Center for Earthquake Studies, The University of Queensland, Brisbane 4072, Australia

Hisao Kanda
National Institute for Materials Science, Namiki 1-1, Tsukuba, Ibaraki 305-0044, Japan

(Received 19 September 2003; accepted 16 January 2004)

High-resolution transmission electron microscopy (HRTEM) was used to study the olivine to spinel transformation. HRTEM structure images of Mg_2GeO_4 olivine deformed under a pressure of 6 GPa at 600 °C clearly show that a shear mechanism dominates the transformation. The transformation is not a nucleation and growth mechanism. It also differs in certain crucial aspects from the type of martensitic transformation proposed before. During the transformation, it is a shear movement that brings the oxygen anions to their positions in the spinel structure. An edge dislocation following each shear then puts the cations in their spinel sites. The Burgers' vector of each dislocation is perpendicular to the anion shear direction. © *2004 American Institute of Physics.*
[DOI: 10.1063/1.1675939]

Olivines have the general formula A_2BX_4 (A and B are cations; X is an anion). They undergo a phase transformation at high pressure and high temperature from the orthorhombic olivine to the cubic spinel-type structure. Many spinels exhibit remarkble electrical, magnetic, and other physical characteristics.[1] The phase transformation of olivine to spinel has also attracted attention among mineralogists, seismologists, geologists, and geophysicists for several decades because of its importance in understanding the earth's mantle dynamics and the origin of deep-focus earthquakes.[2–10] Enormous experimental work on the transformation mechanism has been conducted on both natural olivine and its analogs.[11–24] Two models for this transformation were proposed, i.e., an interface-controlled incoherent nucleation and growth mechanism[3,4] and a dislocation-controlled martensitic mechanism.[5,6] More recently, Chen *et al.*[25] demonstrated that the transformation is a diffusionless anion sublattice transition coupled with short-range diffusional cation reordering. Here we show that a shear mechanism dominates the transformation. The transformation is neither a nucleation and growth mechanism, nor the type of martensitic transformation proposed before.

In the present investigation Mg_2GeO_4 was chosen as an analog for the olivine–spinel transition in mantle silicates.[26,27] The starting material, Mg_2GeO_4 olivine powder (200 mg), was packed in a 7-mm-diam Au capsule. The sample was then placed in a NaCl-10%ZrO_2 pressure medium in a 10-mm-diam graphite heater.[28] The assembly was treated under a pressure of 6 GPa at 600 °C for 10 min using a belt type high pressure apparatus with a 25 mm bore diameter. Thin foils for electron microscopy were prepared from the deformed sample. A JEOL-4010EX HRTEM was used to examine the partially transformed material by taking structure images of very thin specimen areas.

Figure 1 schematically shows the A, B, and C sites of hexagonal close-packed (hcp) and face centered close-packed (fcc) structures. In olivine, the oxygen sublattice possesses the hcp structure and in spinel, the oxygen sublattice possesses the fcc structure. The close-packed plane is $(100)_o$ in olivine and $(111)_s$ in spinel. It can be readily seen from Fig. 1 that in the olivine structure, a shear of the close-packed plane A along any one of the three AC directions will

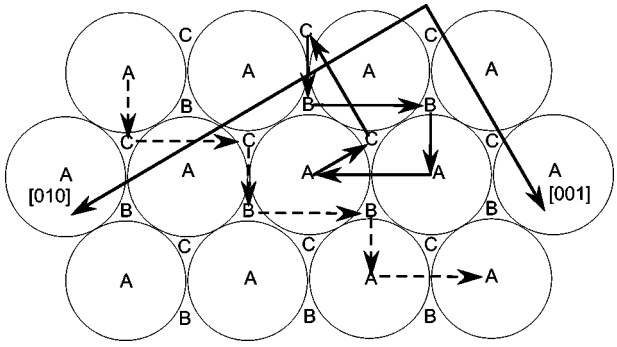

FIG. 1. Schematic representation of the hcp and fcc structures. A plane of close-packed spheres (centered at A) forms the first close-packed plane. The spheres in the second plane can be at either B sites or C sites. If they are at B sites, then the positions of the spheres of the third closed-packed plane can have two choices. They can be either above A sites or above C sites. If they are at B sites, then the sequence is ABABAB···, and the structure is hcp. If the spheres of the third closed-packed plane are at C sites, the sequence is ABCABCABC···, and the structure is fcc. The two arrows labeled with [010] and [001] are the *b* and *c* axes of olivine, respectively. The meanings of other arrows are explained in the text.

[a]Electronic mail: liu.zongwen@nims.go.jp

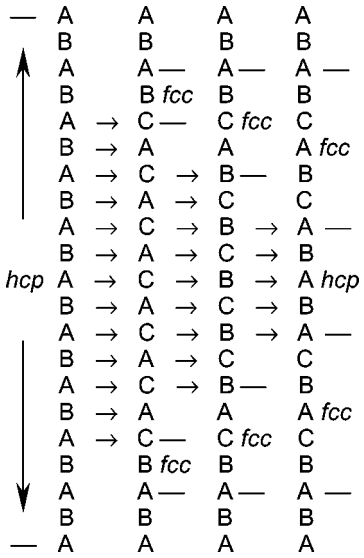

FIG. 2. Schematic representation of the formation of fcc structure from hcp structure through a shear mechanism. The shears occurred on the A, C and B planes, respectively.

lead to a layer, in which the oxygen ions have the fcc (ABC) structure of spinel. When a band of olivine shears like this, two spinel layers will be produced, as shown in Fig. 2. Subsequent shears on every other olivine $(100)_o$ planes will lead to thickening of the layer of spinel. The shear of an amount AC as indicated in Fig. 1 can be easily achieved through gliding of a partial dislocation along AC. Partial dislocations with Burgers's vector $[0\ -1/6\ 0]$ have been observed in $(Mg,Fe)_2SiO_4$ olivine around $MgAl_2O_4$ spinel exsolutions and interpreted as being responsible for the anionic sublattice transformation.[29]

A spinel layer formed in the very early stage of the transformation in our experiment is shown in the middle part of Fig. 3. The orientation is $[0\bar{1}0]_o$ olivine, which is parallel to $[112]_s$ spinel. (Please note that we are using the *Pbnm* space group for olivine's indexes, rather than the *Pnma* space group.) The shear of olivine along $[0\bar{1}0]_o$ (solid arrow AC, Fig. 1) brought the A oxygen anion planes to the C positions. After (or during) the shearing event, the germanium cations moved away from the shear boundary and at the same time some magnesium cations migrated down to the boundary to maintain charge balance. The left-hand side of Fig. 3 clearly shows the state after the oxygen anion shear.

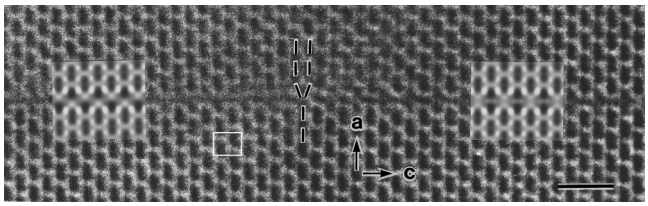

FIG. 3. Structure image of olivine in $[0\bar{1}0]_o$ orientation showing a spinel layer formed by only one shear of olivine along $[0\bar{1}0]_o$ (solid arrow AC, Fig. 1). Each of the black spots corresponds to two germanium atom columns with a spacing of 1.8 Å. An edge dislocation appeared at the center of the image was marked. The two insets are calculated structure images showing both olivine and the spinel layer. The two small arrows show the [100] (*a* axis) and the [001] (*c* axis) directions of olivine and the small white rectangle indicates a unit cell of olivine. The horizontal bar shows the length of two-olivine unit cells along its *c* axis which is about 1.2 nm.

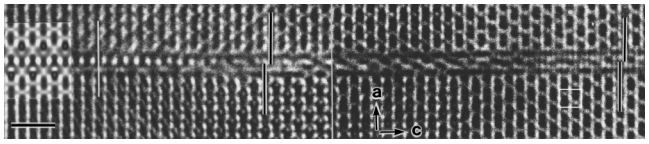

FIG. 4. Structure image in $[0\bar{1}0]_o$ orientation showing both olivine and a layer of spinel formed by two successive shears. The first shear was along $[0\bar{1}0]_o$ (solid arrow AC, Fig. 1) and the second shear was along $[013]_o$ (solid arrow CB, Fig. 1). The right-hand side of the image shows the stage, in which the second edge dislocation has not involved and the cations have not occupied their correct spinel positions. The far left-hand side of the image shows "pure" spinel formed after the involvement of the second edge dislocation (solid arrow BB, Fig. 1). The inset (left) is a calculated image showing both olivine and spinel. The central part of the image was cut off. The two small arrows show the [100] (*a* axis) and the [001] (*c* axis) directions of olivine and the small white rectangle indicates a unit cell of olivine. The horizontal bar shows the length of two-olivine unit cells along its *c* axis which is about 1.2 nm.

However, at this stage, the cations still did not occupy their correct spinel sites. The marked edge dislocation in Fig. 3 (solid arrow CC in Fig. 1) with Burgers' vector $[0\ 0\ -1/2]$, which was gliding in the $[001]_o$ direction (from right to left) on the $(100)_o$ plane, brought the cations to their spinel sites.

To successively form spinel layer by layer, the anion shear must occur on every other plane and the order of the shear sequence is A→C→B→A as shown in Fig. 2. The second shear (from the C plane) moved the C planes to B plane positions. If the olivine grain is compressed evenly from every direction, to minimize the overall shape change, the shear would go along the arrowed CB direction (solid arrow, Fig. 1) rather than the other two CB directions. When viewed along $[0\bar{1}0]_o$ olivine, this second shear caused a shift along $[001]_o$ of one fourth of a unit cell. This is shown in Fig. 4 by the split black lines. Like the first shear, this second shear put the oxygen anions in their spinel positions. The second edge dislocation BB (solid arrow, Fig. 1) at right angles to the CB anion shear then put the cations into their proper spinel positions. The presence of this BB edge dislocation can be easily recognized (see the left-hand side of Fig. 4) as it caused another one-fourth unit cell shift along $[001]_o$. The third shear along the solid arrow BA (Fig. 1) plus the movement of the third associated edge dislocation AA (solid arrow, Fig. 1) would produce another pure spinel layer. After three such shears and the movement of an edge dislocation following each shear, the sheared (untransformed) olivine returned to its initial position. Subsequent shears would repeat the above three shear processes. High-resolution transmission electron microscopy (HRTEM) images involving three and four shears are shown in Fig. 5.

In the absence of a deviatoric stress and with significant restraint on overall shear displacement, there are a number of combinations of shears and dislocations that can result in the formation of three layers of spinel with no overall shear. The solid arrows in Fig. 1 show only one of the many possibilities for this zero overall shear. A transformation that occurs in such a manner is not a classic martensitic transformation, as it results in a negligible (or zero) deviatoric component of the shape change.

However, under anisotropic conditions, such as in the presence of imposed deviatoric stresses, the shears can occur in the same direction. The cumulative effect of these shears

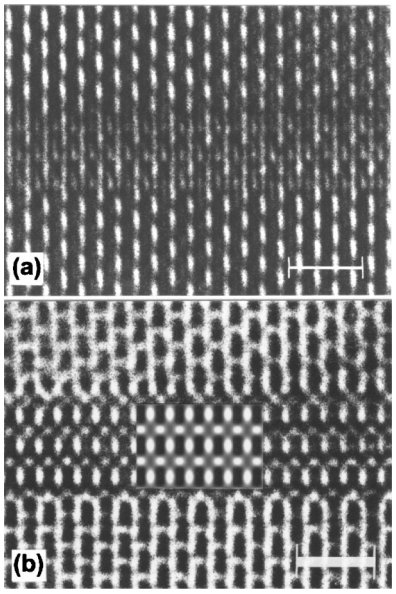

FIG. 5. TEM images in $[0\bar{1}0]_o$ orientation showing spinel layers formed through the shear mechanism. (a) High resolution image showing a spinel layer formed after three shears. (b) Structure image showing a spinel layer formed by four shears. The inset is a calculated image of spinel. Scale bar=1.2 nm.

and their associated dislocations would allow considerable overall shear displacement in the transformed region. The dashed arrows in Fig. 1 show such a sequence of shears and the dislocations involved. If the transformation proceeds in this fashion, leading to a significant change in shape of the transformed region, then it is more legitimately termed martensitic.

It should be mentioned here that it is nearly impossible to achieve ideal isotropic (hydrostatic) conditions experimentally. The starting material we used is a loose powder. It is believed that cold compression of a loose power at 6 GPa generates very high differential stress within the powder. We have observed that some olivine grains were unevenly compressed by their neighbor olivine grains even though the gold capsule was isostatically compressed from every direction by the NaCl pressure medium. In such a case, the spinel bands pushed well into other olivine grains indicating that the shears occurred in a dominated direction. Besides, the olivine-spinel volume change itself also generates high stresses at low temperature as has been observed by Raterron *et al.*[30]

The shear mechanism found in our study is significantly different from the type of martensitic mechanism predicted previously. Poirier[5,6] suggested that dislocations with Burger's vector $[001]_o$ gliding on the $(100)_o$ closed-packed plane can be split according to

$$[001]_o \rightarrow \tfrac{1}{12}[013]_o + \tfrac{1}{12}[0\bar{1}3]_o + \tfrac{1}{12}[013]_o + \tfrac{1}{12}[0\bar{1}3]_o . \quad (1)$$

The stacking fault between the $\frac{1}{12}[013]_o$ and $\frac{1}{12}[0\bar{1}3]_o$ partials can be regarded as a layer in which the oxygen ions have the cubic close-packed structure of spinel. Poirier further proposed that the cations can go to the appropriate sites of the spinel structure by shuffling motions over no more than one atomic distance (synchroshear). The $\frac{1}{12}[013]_o$ and $\frac{1}{12}[0\bar{1}3]_o$ vectors are shown in Fig. 1 by the dotted arrows AC and CA, respectively. The present HRTEM structure images of Mg_2GeO_4 clearly show that while the shear movement brings the oxygen anions to their positions in the fcc structure, it is an edge dislocation following each shear rather than a simple synchroshear motion that puts the cations in their spinel sites. The Burgers' vector of each dislocation is perpendicular to the anion shear direction. It is possible that a transformation nucleated by shear in this way may continue to grow by reconstructive diffusional processes, but so far this has not been observed.

The authors would like to thank Professor Ken Collerson for his helpful view of the manuscript. The work was supported by an Australian Research Council (ARC) large grant. The authors are most grateful for this support. The authors also wish to thank the Diffraction Group, School of Physics at the University of Melbourne for allowing us to use the MUM (Melbourne University Multislice algorithm package) program developed by the Diffraction Group for HRTEM image simulation.

[1] N. W. Grimes, Phys. Technol. **6**, 22 (1975).
[2] P. W. Bridgman, Am. J. Sci. **243A**, 90 (1945).
[3] C. Sung and R. G. Burns, Tectonophysics **31**, 1 (1976).
[4] C. Sung and R. G. Burns, Earth Planet. Sci. Lett. **32**, 165 (1976).
[5] J. P. Poirier, Phys. Earth Planet. Inter. **26**, 179 (1981).
[6] J. P. Poirier, *Anelasticity in the Earth*, Vol. 4 of Geodynamics Series, edited by F. D. Stacey, M. S. Patterson, and A. Nicholas (American Geophysical Union, Washington, DC, 1981), pp. 113–117.
[7] C. Frohlich, New Sci. **148**, 42 (1995).
[8] T.-C. Wu, W. A. Bassett, P. C. Burnley, and M. S. Weathers, J. Geophys. Res. (Solid Earth) **98**, 19767 (1993).
[9] H. W. Green, Sci. Am. **271**, 64 (1994).
[10] S. H. Kirby, S. Stein, E. A. Okal, and D. C. Rubie, Rev. Geophys. **34**, 261 (1996).
[11] P. C. Burnley, W. A. Bassett, and T.-C. Wu, J. Geophys. Res. (Solid Earth) **100**, 17715 (1995).
[12] P. C. Burnley and H. W. Green II, Nature (London) **338**, 753 (1989).
[13] L. Kerschhofer, T. G. Sharp, and D. C. Rubie, Science **274**, 79 (1996).
[14] D. C. Rubie and P. E. Champness, Bull. Mineral. **110**, 471 (1987).
[15] P. J. Vaughan, H. W. Green II, and R. S. Coe, Nature (London) **298**, 357 (1982).
[16] P. J. Vaughan, H. W. Green II, and R. S. Coe, Tectonophysics **108**, 299 (1984).
[17] I. Martinez, Y. B. Wang, F. Guyot, R. C. Liebermann, and J. C. Douhan, J. Geophys. Res. (Solid Earth) **102**, 5265 (1997).
[18] Y. Wang, I. Martinez, F. Guyot, and R. Liebermann, Science **275**, 510 (1997).
[19] K. Fujino and T. Irifune, *High-Pressure Research: Application to Earth and Planetary Sciences* (Terra Scientific, Tokyo/American Geophsical Union, Washington, DC, 1992), pp. 237–243.
[20] A. R. Remsberg, J. N. Boland, T. Gasparik, and R. C. Liebermann, Phys. Chem. Miner. **15**, 498 (1988).
[21] J. N. Boland and L. Liu, Nature (London) **303**, 233 (1983).
[22] N. Hamaya and S. Akimoto, Phys. Earth Planet. Inter. **29**, 6 (1982).
[23] N. Hamaya and S. Akimoto, in *High-Pressure Research in Geophysics*, edited by S. Akimoto and M. H. Manghnani (Center for Academic Publications Japan, Tokyo, 1982), pp. 373–389.
[24] A. Lacam, M. Madon, and J. P. Poirier, Nature (London) **228**, 155 (1980).
[25] J. Chen, D. J. Weidner, J. B. Parise, M. T. Vaughan, and P. Raterron, Phys. Rev. Lett. **86**, 4072 (2001).
[26] A. E. Ringwood, Am. J. Sci. **254**, 707 (1956).
[27] A. E. Ringwood, Geochim. Cosmochim. Acta **13**, 303 (1958).
[28] M. Akaishi, H. Kanda, and S. Yamaoka, J. Cryst. Growth **104**, 578 (1990).
[29] P. Raterron, F. Bejina, J. C. Doukhan, and O. Jaoul, Phys. Chem. Miner. **25**, 485 (1998).
[30] P. Raterron, J. Chen, and D. J. Weidner, Geophys. Res. Lett. **29**, 36-1 (2002).